Magnetic domain wall coercivity and aftereffect in antiferromagnetic/ferromagnetic bilayers

J. Moritz*
Institut Jean Lamour, UMR 7198 CNRS, Université de Lorraine, Bd des Aiguillettes, BP 70239, F-54506 Vandoeuvre-les-Nancy Cedex, France

P. Bacher
ESSTIN, Université de Lorraine, 2, rue Jean Lamour, F-54519 Vandoeuvre-les-Nancy Cedex, France

B. Dieny
Univ. Grenoble Alpes, INAC-SPINTEC, F-38000 Grenoble, France;
CEA, INAC-SPINTEC, F-38000 Grenoble, France; and CNRS, SPINTEC, F-38000 Grenoble, France
(Received 21 March 2014; published 29 July 2014)

Exchange bias and coercivity are investigated in antiferromagnetic (AFM)/ferromagnetic (FM) bilayers by steepest descent and Monte Carlo simulations. For a given range of the AFM anisotropy, a magnetic domain wall parallel to the interface is created in the AFM layer. This domain wall propagates along the AFM thickness and eventually gets pinned at the negative saturation due to the intrinsic Peierls potential of the AFM material. We demonstrate that this pinning and its associated dissipation is one possible source of coercivity in such exchange coupled bilayers. Monte Carlo simulations were also carried out to investigate the influence of thermal fluctuations, which induce a random walk of the domain wall throughout the AFM layer, leading to magnetic aftereffect. Depending on the experimental characteristic measurement time and temperature, the domain wall can eventually be expelled from the AFM layer leading to the reversal of the entire AFM spin lattice. This contribution to the exchange bias phenomenon particularly explains quite well the enhancement of coercivity in exchange coupled bilayers at low temperature, even in polycrystalline samples.

DOI: 10.1103/PhysRevB.90.024429 PACS number(s): 75.50.Ee, 75.60.Ch, 75.70.Cn

I. INTRODUCTION

Exchange bias refers to the shift of the hysteresis loop that arises in ferromagnetic/antiferromagnetic (FM/AFM) bilayers when the system has been cooled down from above the AFM order temperature (T_N) under a large external field. It was discovered in the 1950s [1] and has been extensively studied since then, especially because it has found important technological applications in spintronic devices [2]. In the simple model due to Meiklejohn and Bean [3], which is based on uncompensated (all spin aligned) FM/AFM interfaces, the predicted bias field is several orders of magnitude larger than those experimentally observed. During the past decades, several other models were proposed in the attempt to get better quantitative agreement with experimental data. Models were also developed to explain the origin of the hysteresis field shift (H_{EX}) in the case where the FM/AFM interface is fully compensated (see topical reviews [4–7]). All these models emphasize a particular aspect of exchange bias: e.g., influence of micromagnetism, interfacial disorder, dilution in the antiferromagnet. They all contributed progressing towards a qualitative and quantitative understanding of the exchange bias phenomenon.

First Néel, then Mauri, assumed that the exchange energy cost at the FM/AFM interface, when the magnetization of the FM layer is reversed, is spread over several AFM atomic planes, leading to the formation of a planar magnetic domain wall (DW) in the AFM layer, parallel to the interface [8,9]. Malozemoff showed that the atomic roughness may reduce the exchange bias and calculated in a random field model that H_{EX} is proportional to the DW energy, leading to a similar result as Néel and Mauri [10]. Other authors have numerically studied the effect of interfacial disorder, or exchange interactions, using Monte Carlo calculations, to explain the amplitude of H_{EX} in compensated AFM material where no net magnetic moment exists at the interface [11–13]. In the same compensated spin array, Koon demonstrated the possibility of a biquadratic coupling between the FM and AFM moments which could lead to a hysteresis field shift [14]. His assumption was contradicted by Schulthess and Butler who carried out micromagnetic simulations showing that fully compensated flat interfaces induce a uniaxial anisotropy rather than a unidirectional anisotropy [15]. Besides these previous approaches, which mainly focus on FM/AFM interfacial effects, Nowak and collaborators have studied the influence of disorder and defects in the AFM bulk by using Monte Carlo simulations. They showed that these defects can lead to the formation of magnetic domains in the AFM layer [16]. These domains, frozen during the field cooling procedure, develop a net magnetization at the FM/AFM interface. The authors obtained realistic amplitudes of H_{EX} and could reproduce some characteristics of the exchange bias phenomenon such as its AFM thickness dependence and training effect. They have concluded that a diluted AFM material behaves like a spin glass, which has been inferred by other authors to explain the low temperature increase of H_{EX} and of the dissipation measured in real systems [17,18]. It has also been suggested that the polycrystalline character of FM/AFM thin films could lead to magnetic aftereffect in the AFM layer. In the Fullcomer and Charap model, the exchange bias field is due to the AFM grains that are thermally stable during a hysteresis loop, while the coercivity is associated with the unstable ones [19]. This grain model was successfully used and extended by O'Grady

*jerome.moritz@univ-lorraine.fr

and collaborators to interpret exchange bias in FM/IrMn bilayers [20]. Exchange coupling between AFM grains has also been inferred as a source of exchange bias and training in fully compensated AFM layers by Suess *et al.* [21].

Concerning more specifically the coercivity, a few models besides the granular approach explained above have tried to point out the main sources of dissipation in FM/AFM bilayers based on interfacial frustration or partial domain wall in AFM grains [22–24]. As a matter of fact, the dissipation in AFM/FM bilayers is always larger than the coercivity of the single FM layer. Moreover, its thermal dependence shows a peak just below the blocking temperature (T_B), where the bias field vanishes, as well as a pronounced increase at low temperature. This general behavior is observed with a wide variety of AFM materials [22,25–27]. However, despite the large number of models which have addressed the exchange bias phenomenon, the coercivity mechanism in such systems is still not fully understood, particularly the large coercivity enhancement often observed at low temperatures.

We have recently demonstrated that another contribution to the coercivity in AFM/FM bilayers can arise from the influence of Peierls potential on the propagation of a planar domain wall in the AFM bulk. Our model extends the approach initially proposed by Néel, then Mauri, based on the formation of a magnetic DW in the AFM layer parallel to the interface during the descending branch of the hysteresis loop. We showed that the winding and unwinding of the DW are not reversible processes because of the Peierls potential associated with the atomic lattice in these high anisotropy antiferromagnetic materials commonly used for exchange bias (such as IrMn and PtMn). This potential was investigated during the 1970s in permanent magnet materials and was identified as a source of intrinsic DW coercivity [28–30]. In such large anisotropy systems, the DW are very thin, their width (δ) extends over a few interatomic distances, and the DW energy γ varies periodically along the crystal axis as

$$\gamma(z) = \gamma_0 + \frac{\Delta\gamma}{2}[1 + \cos(2\pi z/a)], \tag{1}$$

where $\Delta\gamma = \Lambda J \exp(-\pi\delta/a)$ is the Peierls potential, a the lattice parameter, J the exchange constant, Λ a numerical factor of the order of 10^2–10^4, $\gamma_0 \simeq 4\sqrt{JK}$ the continuous DW energy, and z the coordinate along the DW propagation direction supposed to correspond to a crystal lattice axis. To make the DW center move from one atomic position to the next, the Peierls potential barrier must be overcome, which induces an increase of the coercive field in permanent magnet materials at low temperature [31,32], typically below 50 K, similar to what is observed in FM/AFM bilayers. Taking into account the finite size character of AFM/FM systems and assuming that the torque on the DW is transmitted in a first approximation via the FM/AFM interface only (the susceptibility of the antiferromagnet to the applied field was supposed to be negligible), the following analytical expressions of the critical (coercive) fields were derived [33]:

$$H_1 = -2\sqrt{JK}, \tag{2}$$

$$H_2 = H_1 + \frac{\Delta\gamma}{\tanh\xi n_C - \tanh\xi\left(n_C - \frac{1}{2}\right)}, \tag{3}$$

where n_C is the pinning position of the DW inside the AFM thickness at the negative saturation, $\xi = \sqrt{\frac{K}{J}}$, and $2\sqrt{JK}$ is the half DW energy in the continuous approximation. The bias field H_{EX} and the coercive field H_C are related to these critical fields by $\frac{H_1+H_2}{2}$ and $\frac{H_1-H_2}{2}$, respectively. Furthermore, when the AFM thickness is larger than δ, at negative saturation, the DW center may jump from one minimum of the pseudoperiodic Peierls potential to the next because of thermal activation. As a result, a random walk motion of the DW through the AFM thickness was predicted and thermal expressions of both H_{EX} and H_C were derived. Although our calculations were in good agreement with experimental observations, some opened issues had to be addressed, concerning more particularly the random walk process of the DW and the evolution of the Peierls potential with temperature. Indeed, in our previous work, we assumed phenomenological thermal variations of the magnetic parameters such as K and J, and, consequently, of the DW width. As the Peierls potential drastically depends on them, more realistic calculations were needed in order to investigate whether large DWs can be pinned within the AFM thickness as well as to derive the critical temperature at which the DWs begin to be expelled from the AFM layer as a function of K or J. Applied field sweep rate dependence of the random walk, and, more generally, the training effect due to these thermally activated processes, had to be also studied more carefully.

In this paper, we present numerical simulations (steepest descent and Monte Carlo) performed on an ideal system consisting of an uncompensated AFM layer coupled to a FM material via a perfectly flat interface. In a first part of the paper, the model and algorithms used for the calculations are detailed. In a second part, the results of the steepest descent calculations for different AFM thicknesses are presented. Both athermal H_{EX} and H_C were extracted from the calculated hysteresis loops, as well as the spin configuration in the AFM layer at negative saturation versus AFM anisotropy. Depending on the anisotropy strength, the entire spin array may be reversed, remain frozen, or exhibit a magnetic DW pinned inside the AFM thickness. We explain the role of the AFM anisotropy on the different regimes as well as the importance of the Peierls potential on the depinning process. Finally, in a last part of the paper, we investigate the influence of temperature on the AFM spin configuration by using Monte Carlo simulations. Above a critical temperature, the DW can be expelled out from the antiferromagnet, leading to a large coercivity and no exchange bias. Below this critical temperature, the thermally activated depinning and short distance propagation of the narrow domain wall within the AFM layer yields an increase of the coercive field, consistent with experimental observations.

II. MODEL

We consider in this paper a two-dimensional (2D) noncompensated AFM layer with a flat interface coupled to a FM one with a lattice parameter $a = 1$. The system is composed of 1 FM atomic plane (labeled 0) and N AFM ones (labeled from 1 to N). The AFM layer exhibits a uniaxial anisotropy K, whereas the FM layer, carrying a magnetization $M = 1$, is a soft magnetic material with $K_F = 0$. The exchange constant at the interface is $J_0 = 0.7$ and $J = -0.5$ in the AFM bulk.

Each spin is free to move in the plane only and makes an angle θ_i with the easy axis direction. A set of θ_i angles will be denoted by the "vector" $\vec{\theta}$ in the rest of this paper. The aim of the steepest descent calculations is to follow a local minimum in the total magnetic energy $E(\vec{\theta})$ when the applied field H is decreased from the positive saturation $H_{\rm SAT}$ down to negative saturation $-H_{\rm SAT}$ and then increased back to the final positive saturation so as to simulate a hysteresis loop (the field is applied parallel to the easy axis). The algorithm of the calculations can be described as follows.

(i) An initial configuration of the FM and AFM spins is chosen corresponding to positive saturation under a large external field.

(ii) The field is then decreased by small steps from $H_{\rm SAT}$ down to $-H_{\rm SAT}$. For each field increment, a new spin configuration is derived following the steepest gradient of the total energy. If $\vec{\theta}^{n+1}$ is the new spin configuration to be calculated and $\vec{\theta}^{n}$ the spin configuration of the previous step, $\vec{\theta}^{n+1}$ is given by

$$\vec{\theta}^{n+1} = \vec{\theta}^{n} - \frac{\overrightarrow{\rm grad} E(\vec{\theta}^{n})}{||\overrightarrow{\rm grad} E(\vec{\theta}^{n})||}\delta\theta. \quad (4)$$

If the energy balance $E(\vec{\theta}^{n+1}) - E(\vec{\theta}^{n})$ is negative, then the new spin configuration is accepted. Else, $\delta\theta$ is divided by 10 and the procedure is run once again until the energy balance test is verified. When $\delta\theta$ becomes as small as 10^{-14}, the minimum of energy for the given field step is assumed to be reached. If $\delta\theta$ is small enough, this algorithm avoids energy barriers to be overcome without thermal activation. An initial value of $\delta\theta = 10^{-6}$ was chosen to prevent such an artifact.

In this study, we mainly focused on the effect of the torque exerted by the FM magnetization at the FM/AFM interface on the spin configuration in the AFM layer, as a function of the anisotropy K. That is why any direct coupling between the AFM spins and the external field was neglected in this study. No demagnetization energy was considered either; the spins are only free to rotate in the plane, just as in thin magnetic films due to easy-plane shape anisotropy.

Under these conditions, the total magnetic energy of the system can be written:

$$E = -H\cos\theta_0 - 2J_0\cos(\theta_1 - \theta_0) + \sum_{i=1}^{N} K\sin^2\theta_i - \sum_{i=1}^{N-1} 2J\cos(\theta_{i+1} - \theta_i). \quad (5)$$

Concerning the Monte Carlo (MC) simulations, the same initial configuration is set corresponding to all spins saturated in the positive direction. For each field step, a MC procedure is performed as follows.

(i) A single spin labeled i within the structure is randomly chosen as well as a corresponding tilt $\delta\theta_i$, such as $-\delta\theta(T) < \delta\theta_i < +\delta\theta(T)$, where $\delta\theta(T) = 0.1\sqrt{T}$. Then the energy variation ΔE is calculated as

$$\Delta E = E(...\theta_i + \delta\theta_i ...) - E(...\theta_i ...). \quad (6)$$

(ii) The probability of acceptance of the event is 1 if $\Delta E < 0$, else given by the Boltzmann factor $P = \exp\frac{-\delta E}{T}$.

We performed generally 10^5 iterations per spin and the magnetization for each field increment is averaged only on the last 1000. The same procedure is run from 50 to 800 times depending on temperature. The characteristic fields H_{EX} and H_C are then averaged on all the several hundred stored hysteresis loops.

III. STEEPEST DESCENT RESULTS

Hysteresis loops were calculated for increasing values of the AFM anisotropy and some are shown in Fig. 1 for $N = 25$. We observe three different regimes depending on the anisotropy strength. For high K [Fig. 1(b), $K = 1$], the magnetization reverses reversibly and the loop is completely shifted, just as if a fictive field would maintain the magnetization in the positive direction. For intermediate K values, the loop is still shifted, but some dissipation occurs ($K = 0.343$). And finally, for small K, the hysteresis loop is opened and centered and the system behaves like a hard ferromagnet [Fig. 1(a)].

Surprisingly the variation of coercivity versus anisotropy reported in Fig. 1 is not monotonous on the whole range of AFM anisotropy investigated as shown in Fig. 2. In this reduced K interval, increasing K leads to a reduction of H_{EX} and a slight increase of the dissipation: it is more difficult to saturate the magnetization in the negative applied field direction and to reverse the system back to its initial state when the anisotropy is larger (the ascendant critical field increases with K). Some jumps occur also at small and large applied fields where the magnetization rotates irreversibly (see inset of Fig. 2).

In order to correctly extract both exchange bias and coercive fields, the whole hysteresis loops were numerically computed. H_C was then derived by determining the half loop area by numerical integration. Concerning the exchange bias, the loops were sliced into 100 parts along the magnetization axis and

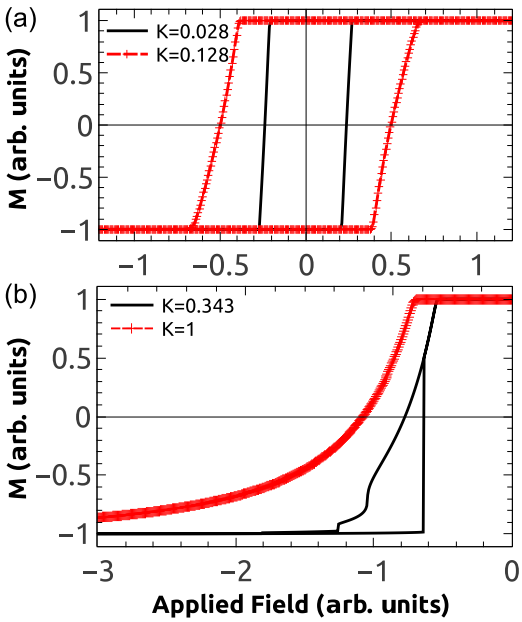

FIG. 1. (Color online) Calculated hysteresis loops using the steepest descent technique for $N = 25$ and different anisotropy values.

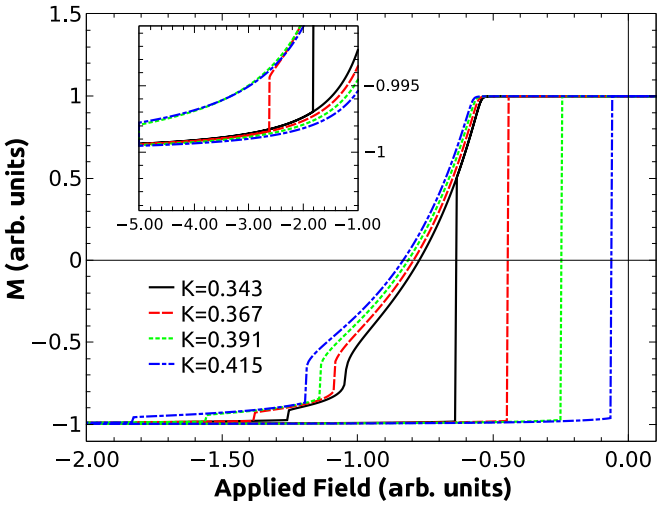

FIG. 2. (Color online) Calculated hysteresis loops using the steepest descent technique for $N = 25$ and increasing anisotropy values. In inset is shown a zoom close to the saturation where irreversible jumps of the magnetization of the order of 0.5% occur at very large field.

H_{EX} averaged on all the slice centers. Using these methods, H_{EX} and H_C were determined for K varying from 0 to 1 by steps of 0.001. Their variations are shown in Fig. 3 for four different AFM thicknesses.

For all thicknesses, below a critical anisotropy value, denoted by K_{DW} in the rest of this paper, the hysteresis loop is centered and the dissipation tends to increase with K. Above K_{DW}, a succession of intervals separated by discontinuities is observed, over which H_{EX} decreases whereas H_C increases, till another critical anisotropy value denoted by K_G. Above K_G, the constant hysteresis loop shift is simply related to the interfacial exchange energy by $2J_0$, while the dissipation completely vanishes. The number of intervals depends on the AFM thickness (12 for $N = 25$, 7 for $N = 15$, 5 for $N = 10$, and 2 for $N = 5$) as well as the critical value K_{DW}. The thicker the AFM layer, the smaller K_{DW} and, then, the larger the intervals number. There is actually a clear correlation between the DW width $\delta = \pi\sqrt{J/K}$ at the critical anisotropy K_{DW} and the total number of AFM planes as depicted in the inset of Fig. 3(b). From this linear relationship, it can be seen that the AFM thickness should be a certain amount of the DW width to be in the pinning regime. To understand the origin of the transition between the two regimes corresponding to a fully dissipative loop (coercivity without loop shift) and a shifted loop (pinning regime), we observed the progression of the spin angles with the applied field for $K = K_{DW}$ and just below (see Fig. 4 for $N = 25$). The angles in Fig. 4 are plotted between 0 and π as if all exchange constants were positive to facilitate the reading. For $K = K_{DW}(0.129)$, the formation of a magnetic DW parallel to the interface is observed. This DW penetrates deeper and deeper to a certain depth within the AFM layer as the applied field increases. At negative saturation, the DW ends pinned with its center between the 12th and the 13th atomic plane. The continuous line in Fig. 4 gives the spin angles with a relatively good agreement using the well-known approximation

$$\theta_i = 2 \arctan \exp \xi[i - n(H)], \tag{7}$$

where $n(H)$ is the DW center position as a function of the applied field H.

Therefore, increasing the field makes $n(H)$ increase from negative values (the DW is outside the AFM thickness) till $n(H) = n_C = 12.5$ at negative saturation, where the DW ends pinned. Now if $K(0.128) < K_{DW}$, the same process occurs but the DW propagates throughout the entire AFM layer without getting pinned [Fig. 4(b)]. In both cases, the energy needed to reverse the magnetization during the descending hysteresis branch is associated with the formation of a magnetic DW.

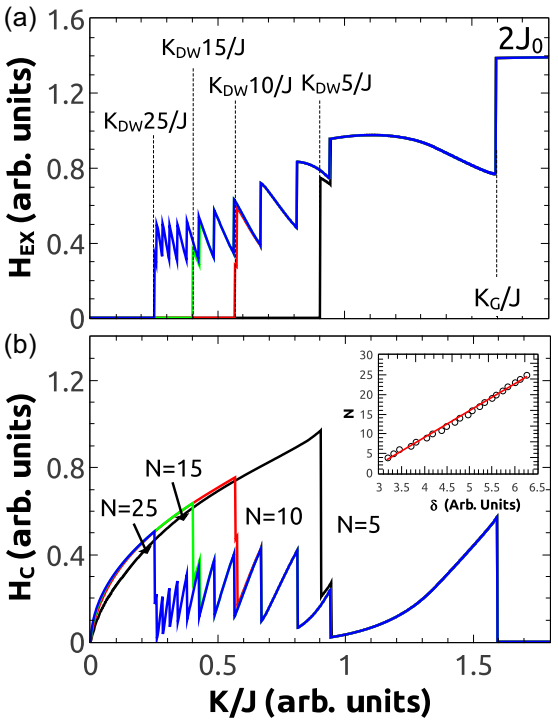

FIG. 3. (Color online) Variation of the exchange bias (H_{EX}) and the coercivity (H_C) with respect to the ratio between the AFM anisotropy K and the exchange energy J, for various AFM thicknesses (N in atomic plane numbers) deduced from the steepest descent calculations. In inset is shown the variation of the AFM thickness N vs the DW width δ at $K = K_{DW}$.

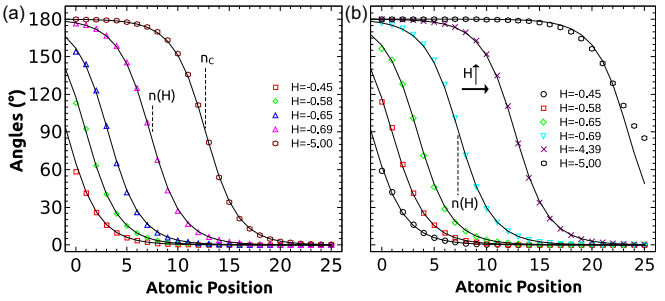

FIG. 4. (Color online) DW progression inside the AFM thickness with respect to the applied field H. The continuous line in the figure are the spin angles calculated in the continuous approximation given by Eq. (7), $n(H)$ being adjusted for each field value. In (a) $K = 0.129$ and the DW is pinned between the 12th and the 13th AFM atomic plane ($n_C \simeq 12.5$). In (b) $K = 0.128$ and the DW is expelled out from the AFM layer when the field is increased.

This energy is provided by the Zeeman coupling between the field and the ferromagnet magnetization and transmitted to the AFM system via the FM/AFM interface. For this reason, the descending coercive field H_1 is given by $H_1 = -2\sqrt{JK}$ expressed in energy units as demonstrated in our earlier study [33]. During the ascending branch though, two different processes can occur, depending on the state which has been reached at negative saturation. If, at negative saturation, the DW is pinned inside the AFM thickness ($K > K_{DW}$), the critical ascending field H_2 is a depinning field. On the other hand, if $K < K_{DW}$, the entire AFM spin array has been reversed by the propagation of the DW throughout the entire AFM layer so that the same symmetric reversal process takes place during the ascending branch leading to $H_2 = -H_1 = 2\sqrt{JK}$. Above K_G, no DW is formed during the descending branch of the hysteresis loop, because this process costs more energy than breaking the interfacial exchange energy only, leading to the absence of dissipation and a bias field of $2J_0$ in energy units.

In Fig. 5, the variation of the DW center position is shown at negative saturation (n_C) with respect to the anisotropy strength for $N = 25$. It exhibits a succession of 12 intervals, similar to the intervals depicted in Fig. 3 for H_{EX} and H_C. Within each interval, the DW center remains located very close to the middle between two AFM atomic planes (i.e., n_C is almost a half integer), where the Peierls potential is minimum. We explained in our previous study that n_C is actually not exactly an half integer because of the finite thickness and dissymmetry of the system [33].

When the AFM anisotropy is increased, the DW center progresses from the middle of the AFM thickness ($n_C = 12.5$ just above K_{DW}) to $n_C = 1.5$, close to the FM/AFM interface. For this particular range of anisotropy ($0.48 < K < K_G$), where $n_C = 1.5$, the DW is of an atomic distance width, which corresponds to the largest H_{EX} and H_C in the DW regime ($K/J > 1$). In the inset of Fig. 5(a), a sketch of the spin configuration in the minimum of the Peierls potential is shown for $K = 0.343$ ($n_C \simeq 3.5$). The central spins of the DW are tilted respectively to the hard axis, corresponding to the lowest energy case. The DW center does not slip into the next minimum available (here in $n_C \simeq 2.5$), because $\theta_0 \simeq \pi$ so that there is not enough Zeeman torque available for the DW to overcome the next Peierls barrier. It is also important to notice that just before the negative saturation, some irreversible jumps in the hysteresis loops occur at large field as illustrated in Fig. 2. This is due to the small angle deviation ($\theta_0 - \theta_1$) at this stage, which reduces the efficiency of the torque transmitted to the AFM layer, so that a large applied field is required to overcome the few last Peierls barriers and reach the final position n_C.

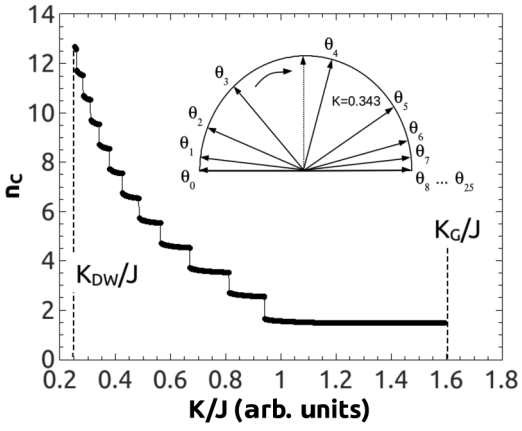

FIG. 5. Variation of the DW center position n_C versus the ratio between the anisotropy K and the exchange energy J. In inset is shown a sketch of the atomic spin angles for $K = 0.343$ at the negative saturation. When one of the central spin (here $i = 3$) is perpendicular to the easy axis, the total magnetic energy is maximum. The amount of energy needed to reach this metastable state from the equilibrium position at the saturation is the depinning energy.

The unwinding of the DW from this equilibrium position is achieved during the ascending branch of the hysteresis loop when the central spin of the DW is brought perpendicular to the easy axis at the maximum of the Peierls potential (the third spin in the inset of Fig. 5). The amount of energy required to achieve such configuration of the magnetic moments defines the DW coercivity. This depinning process is similar to what has been inferred in hard permanent magnet. In most of the available analytical models, the DW angles are supposed to always follow the variation given by Eq. (7); when the DW undergoes a displacement under the external field pressure, along the crystallographic axis, its energy [the last two terms of Eq. (5)] oscillates with the crystal period [each time the central spin is perpendicular (tilted) with respect to the easy axis the energy is maximum (minimum)]. This simple reasoning has allowed the calculation of H_2 [see Eq. (3)] in our previous paper except that the torque of the applied field was transmitted through the FM/AFM only in a first approximation. As a matter of fact, the steepest descent calculations performed in this study corroborate the assumption made on the DW spin angles variation (for any applied field value, when $K/J < 1$, the arctan profile is still valid as shown in Fig. 4) and numerically evidence the Peierls potential oscillating character. We have not considered in our calculations, as explained previously, the coupling between the external field and the AFM spins in order to focus on the transmission of the field torque via the AFM/FM interface. We showed just above that, even for small K, a DW can be trapped in a potential well, as long as the DW width is of the same order of magnitude as the AFM thickness. However, the AFM susceptibility assumed here as negligible could be large enough in such situation to drag the DW out of the AFM layer. The coupling between the applied field and the AFM central spins at the DW core may be sufficient to overcome the reduced Peierls potential in this low anisotropy range (its strength drastically depends on the δ/a ratio). The requested field to achieve such depinning is of the order of $\frac{\Delta\gamma}{S}$, where S is the magnetic moment per AFM atom, which has to be compared with the nucleation field in the DW regime, i.e., $\frac{\sqrt{JK}}{M}$ (the field required to create the DW). Assuming, for instance, the total FM magnetization being $M = 20 \times S$, both fields are of the same order of magnitude for $K/J < 0.8$; then, for such low anisotropy values, the coupling between the external field and the AFM spins has to be taken account and this can qualitatively change the results presented in the first part of this paper.

IV. MONTE CARLO SIMULATIONS

To investigate the influence of temperature on the different processes explained above during both ascending and

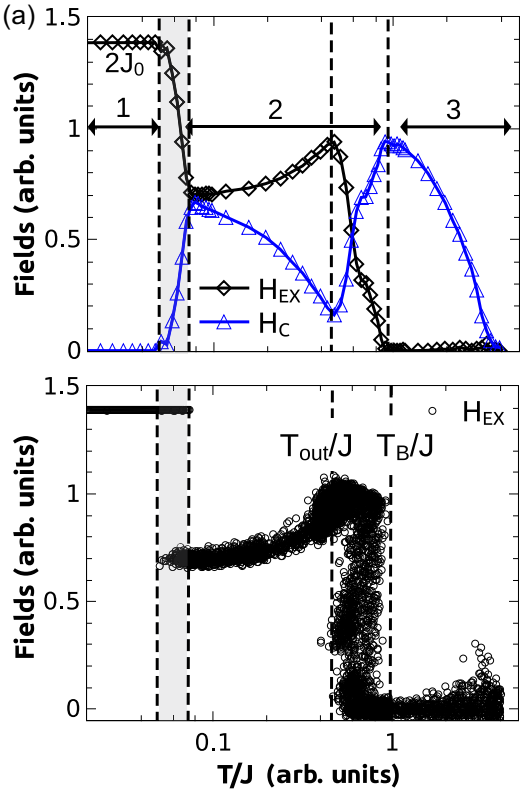

FIG. 6. (Color online) (a) Averaged characteristic fields extracted from the MC simulated loops for $N = 25$ and $K(0) = 0.9$. Both exchange bias (H_{EX}) and coercive field (H_C) exhibit three different regimes with respect to T/J. (b) H_{EX} extracted from all individual hysteresis loops with respect to T/J. The gray shaded region in both graphics delimits the transition between the first and the second regime.

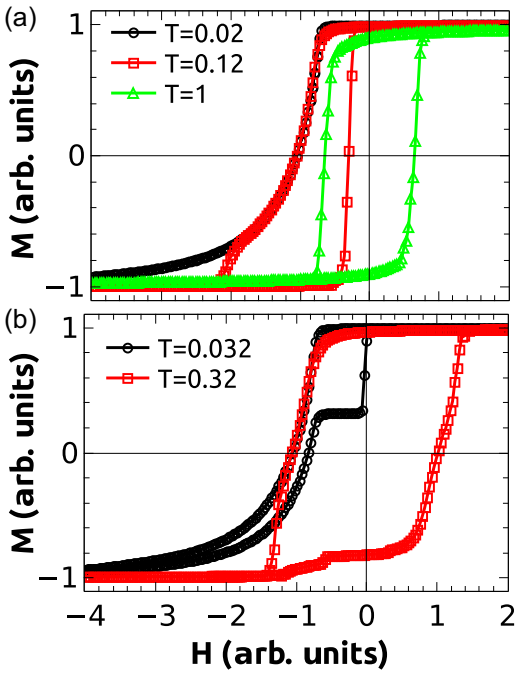

FIG. 7. (Color online) Averaged hysteresis loops extracted from the MC simulations at different temperatures.

descending hysteresis branches, Monte Carlo simulations were performed. We used the same exchange parameters ($J = -0.5$ and $J_0 = 0.7$) as for the steepest descent calculations, the AFM thickness is $N = 25$, and we set the anisotropy value to $K = 0.9$ in order to have $K > K_G = 0.82$ at $T = 0$. Note that the magnetic parameters do not vary with temperature and are kept constant during the calculations. In Fig. 6, the averaged thermal variations of H_{EX} and H_C are shown (each value is averaged on all the loops calculated with the MC method). Three regimes (1, 2, and 3) can be seen for $T < 0.024$, $0.038 < T < 0.48$, and $T > 0.48$. By comparing these results with the curves H_{EX} and H_C vs K shown in Fig. 3 and analyzing the spin angles during the hysteresis loop, we can associate the three regimes with a reversal mode of the spins in the AFM layer.

For $T < 0.024 \simeq J/20$, the spin configuration in the antiferromagnet remains unchanged during the hysteresis loop. When the FM magnetization switches, the exchange energy is all accumulated at the FM/AFM interface (as an atomically thin DW), giving rise to a maximum exchange bias of $2J_0 = 1.4$ and no dissipation (similar to $K > K_G$ in Fig. 3). The average hysteresis loop plotted in Fig. 7(a) calculated at $T = 0.02$ is very similar to the one shown in Fig. 1(b) obtained with the steepest descent method for $K = 1 > K_G$. In the second regime, there is first an increase of the exchange bias from $T = 0.038$ up to $T = T_{\text{out}} = 0.24 \simeq J/2$, and then a decrease up to $T = T_B = 0.48 \simeq J$ where it vanishes. For $0.038 < T < T_{\text{out}}$, the average hysteresis loop shape looks like the one calculated with the steepest descent technique in the DW pinning regime [see Fig. 7(a) for $T = 0.12$ and compare with Fig. 1(b)]. On the other temperature range though, for $T_{\text{out}} < T < T_B$, the average computed hysteresis loop is a statistical mixing between a DW pinning regime, leading to exchange bias and coercivity, and an opened centered loop inducing high coercivity only. A statistical mixing is also seen in the transition region between the first and the second regime, for $0.024 < T < 0.038$, where the average hysteresis loop is a superposition of both adjacent regimes [see Fig. 7(b) for $T = 0.032$]. Finally, in the third regime, the hysteresis loop is centered only and its area decreases with increasing temperature [see Fig. 7(a) for $T = 1$].

In Fig. 8(a), the DW profiles at $T = 0.2 < T_{\text{out}}$ are shown for different applied field values up to the negative saturation for a single computed hysteresis loop [the corresponding loop is plotted in Fig. 9(a)]. The DW is of an atomic distance width but its center position n_C varies with the external field. As shown in Fig. 9(b), the DW center undergoes a random walk through the AFM thickness. Its center position does not exceed 5.5 atomic layers in the AFM depth, much below the actual AFM thickness. During the ascending hysteresis branch, the DW gets unpinned at the ascendant critical field $H_2(T)$, leading to both exchange bias and coercivity.

At a given temperature, in the Monte Carlo procedure, each calculated loop yields a different maximum penetration depth of the DW inside the AFM layer. This maximum penetration depth however never exceeds the total AFM thickness as long as $T < T_{\text{out}}$. Above this critical temperature though, the maximum penetration depth increases so that the DW

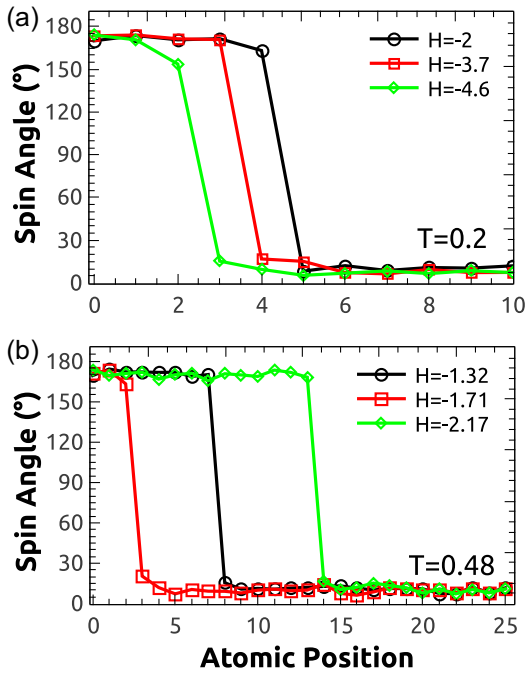

FIG. 8. (Color online) DW profile as a function of applied field at $T = 0.2$ (a) and $T = 0.48$ (b).

can sometimes get expelled out of the AFM layer during its random walk. This effect gets more and more frequent as the temperature increases up to $T = T_B = 0.48$, above which the maximum penetration depth becomes always larger than the AFM thickness. Above this blocking temperature, the DW is still sharp [see Fig. 8(b)] but the random walk always brings the DW out of the AFM layer (so that it annihilates) during the descending branch of the hysteresis loop. The same process arises during the ascending branch, leading to the absence of exchange bias and a large coercivity [see Figs. 9(c) and 9(d)]. Moreover, for $T_{\text{out}} < T < T_B$, there is a large distribution of the exchange bias values extracted from the individual hysteresis loops because of the large distribution of the maximum penetration depth [see Fig. 6(b)]. The deeper the DW at $-H_{\text{SAT}}$, the larger the dissipation and the smaller the exchange bias in average in this regime.

Finally, when the temperature is further increased above T_B (third regime), the same process as described above arises with a sharp DW moving throughout the AFM lattice. The higher the temperature, the shorter the transit time of the DW throughout the AFM layer. Barbara showed that when the ratio $K/J > 4/3$ in the context of hard permanent magnets, the magnetic DWs are Ising type walls of an atomic distance width [34,35]. The K/J ratio at $T = 0$ here is of 1.8, larger than the critical ratio calculated by Barbara, so our results are consistent with his assumption and calculations. When the temperature is taken into account though, the DW width may change. Lajzerowicz and Niez calculated a phase diagram giving the DW type (Bloch or Ising) in the $(T, K/J)$ space [36]. According to their calculations, when $K/J > 4/3$, the DW is always in the Ising regime whatever the temperature, which is also consistent with our observations. In the scenario explained above, the DW undergoes a random walk within the AFM layer when the magnetization is at negative saturation. In this configuration, $\theta_0 \simeq \theta_1 \simeq \pi$ and no more Zeeman torque is transmitted to the AFM system via the FM/AFM interface, even if the applied field is still increased. To make the DW progress from one atomic position to another, the Peierls potential has to be overcome, which is achieved here by thermal activation only. This process leads to a magnetic DW aftereffect in the AFM layer where time is, of course, another key parameter. If the total time during which the FM magnetization remains saturated in the negative direction is reduced in the calculations presented in Fig. 9(c), for instance, by decreasing the saturation field or the total number of iterations per field step (i.e., the applied field sweep rate), the DW may not be expelled out of the AFM layer which would result in an open and shifted hysteresis loop.

In order to study such time effect on H_{EX} and H_C vs T characteristics, we varied the total iterations number per field step for $N = 25$ (see Fig. 10). The same three regimes as previously reported are seen in Fig. 10 with different thermal ranges.

The blocking temperature T_B and the critical temperature T_{out} increase as the number of iterations is decreased (meaning that the applied field sweep rate increases). Actually, when the number of iterations is decreased, the number of steps in the random walk is reduced, and so is the probability for the DW to get expelled out of the AFM layer. This reinforces in fine the DW pinning regime and shifts all characteristics fields to higher temperatures. The exchange bias amplitude at the beginning of the second regime decreases also with the number of iterations (i.e., the depinning process costs more energy and the dissipation increases). This is also due to the reduced role of thermal activation at shorter time in the DW depinning process. Then, when the applied field sweep rate is increased, the exchange bias can be enhanced or reduced, depending on the calculation temperature. This is again associated with the reduced role of thermal activation at shorter time scale, making the depinning process more difficult. Experimentally, both tendencies have been measured on different systems, i.e., an enhancement [37] or a reduction [38,39] of the exchange bias with the applied field sweep rate, which could be explained by this DW aftereffect in the AFM layer.

Before concluding, let us emphasize that the model presented in this paper has been developed in the ideal case of perfectly flat interfaces and single crystal AFM material. The purpose of choosing this ideal structure was to clearly demonstrate the influence of the Peierls potential in the loop shift and coercivity of exchange bias systems. In realistic polycrystalline exchange bias systems, the described phenomena may still be present at the scale of each individual AFM grain. The common interpretation of loop shift and coercivity in exchange bias systems in the granular model of Fulcomer and Charap [19] and later O'Grady *et al.* [17] consists in associating the loop shift to the stable AFM grains and the coercivity to the unstable ones. In this paper, we show that because of the irreversible propagation of DW within the AFM grains due to the Peierls potential, even the stable grains can contribute to the coercivity. Moreover, grains which would have been considered as stable within a granular model could behave as unstable using ours. In the granular approach, the barrier height preventing the AFM spin reversal is related to the bulk anisotropy which

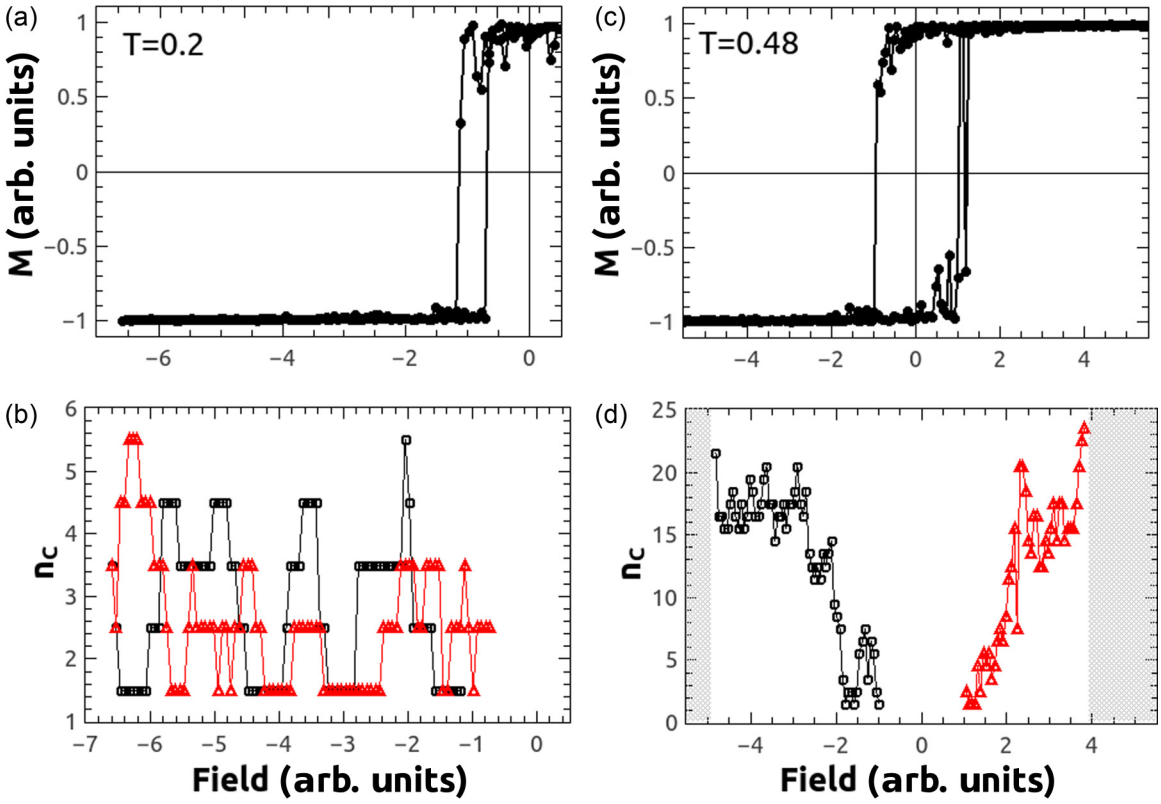

FIG. 9. (Color online) (a) Single hysteresis loop calculated at $T = 0.2$. (b) Progression of the DW center with the applied field at $T = 0.2$ for the particular hysteresis loop shown in (a). (c) Single hysteresis loop calculated at $T = 0.48$. (d) Random walk of the DW center for the loop shown in (c). The shaded area corresponds to the field ranges where the DW has been expelled out from the AFM layer.

counterbalances the torque at the interface exerted by the magnetization: in other words, all AFM spins should rotate coherently to achieve the entire grain reversal. In our approach, the same process arises from the random walk of the DW throughout the AFM layer and the barrier height separating two minima of the Peierls potential is lower than the one calculated with a granular model (only a few spins rotate in this case). It is then easier to reverse the AFM spin array by several jumps of the DW through the periodic Peierls potential by thermal activation; that is why the stability criterion differs from one model to the other and why grains with high anisotropy can become unstable in our model. Moreover, although our model deals with a perfect single crystal system, the polycrystalline character of realistic samples could be taken into account by assuming, for each grain, an effective interfacial coupling whose amplitude would depend on the grain diameter like in Takano's study [40]. Such distribution of J_0 would induce a distribution of K_G and a spreading of the second regime (one atomic distance DW depinning regime) shown in Fig. 6. The presence of atomic roughness at the FM/AFM interface, and more generally of defects in the AFM layer, is also known to create magnetic frustration and can lead to the formation of AFM domains, or bubbles in the AFM bulk, as explained in Refs. [10,16]. The same reasoning that we had for horizontal DWs, parallel to the interface, would be also valid for vertical or partial DW delimiting AFM domains of different orientations. So the Peierls potential would be a source of irreversibility in such complicated magnetic structure that could induce a spin-glass-like behavior.

Finally, for comparison with experimental data, we can try to rescale the calculated fields given in Fig. 6 with experimental values. The calculated T_B where H_{EX} vanishes is of about 0.50 expressed in arbitrary units. In IrMn, for instance, the blocking temperature is of the order of 500 K [25], so that room temperature in Fig. 6 would correspond to ∼0.30. Accordingly, the second regime would take place in the temperature range ∼30–300 K, while the perfect spring regime (regime 1 in Fig. 3) would occur at even lower temperature <25 K. Assuming an interfacial exchange energy J_0 of the order of 1 meV (see [16,21,41]), a lattice parameter of 0.4 nm, and a FM layer consisting of a 10 nm Co thin film, the corresponding H_{EX} would be of about 360 Oe at room temperature, 720 Oe at 30 K, and 1400 Oe at 0 K. These amplitudes and increase of the bias field with decreasing T are consistent with experimental measurements. Note that the ratio K/J at T_{out} is of about 1, which means that only very sharp DWs can be pinned inside the Peierls potential. This stability criterion can eventually be derived by assuming the DW undergoes about N^2 Peierls barrier jumps before being expelled out of the AFM layer. In these random walk conditions, the barrier height should be of the order of $\ln(\frac{t}{N^2\tau_0})$, which leads, with t in the minute range, $\tau_0 = 10^{-9}$ s, and $N = 25$, to 18 kT (k is the Boltzmann constant and T the absolute temperature). Within a grain of diameter d, the Peierls barrier height is of about

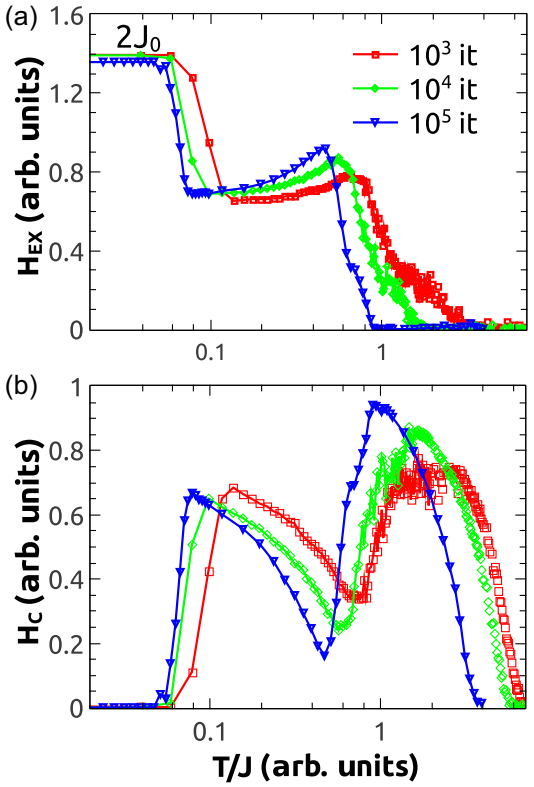

FIG. 10. (Color online) Variation of the characteristic fields H_{EX} in (a) and H_C in (b) with respect to T/J and for different iteration number per spin.

$\frac{d^2}{a^2}\Lambda J\Delta\gamma$, giving a ratio $K/J = 1.31$ to ensure the DW will not be expelled from the AFM layer during the experimental time (using $T = 300$ K, $d = 15$ nm, and $J = 1$ meV). This is clearly consistent with our Monte Carlo simulations. The AFM anisotropy can be evaluated in this DW regime using the same lattice parameter as previously where $J \simeq K$ to 2.5×10^6 J/m^3, close to what is measured in IrMn alloys [19,42,43].

V. CONCLUSION

In this paper, we have numerically studied the magnetization reversal in a FM/AFM bilayer of finite thickness with ideally flat uncompensated interface. The steepest descent calculations showed that during the descending branch of the hysteresis loop, there is formation of a magnetic domain wall parallel to the interface in the AFM thickness as long as the energy cost to form this magnetic structure is lower than the interfacial exchange energy. The formation of such magnetic wall at the negative saturation has been inferred years ago by Néel and Mauri. Unlike their initial assumptions, the winding/unwinding of the DW is not a reversible process because of the Peierls potential which arises in these high anisotropic AFM materials. We showed actually that, depending on the anisotropy strength, the DW can get pinned inside the AFM thickness. The larger the AFM anisotropy K, the closer to the FM/AFM interface is the DW center at negative saturation. The depinning field H_2 is determined by the Peierls potential which has to be overcome to bring the system back to its initial state during the ascending hysteresis loop branch. By using Monte Carlo simulations, we showed that a random walk process of the DW takes place within the AFM layer. If the calculation time is large enough, the DW can be expelled out of the AFM layer. The same process then takes place symmetrically during the ascending hysteresis branch leading to a large coercivity and no exchange bias. On the other hand, if the DW is still present in the AFM layer during the ascending branch, there are both exchange bias and dissipation. The DW undergoes magnetic aftereffects where the combination of time and temperature can lead to different magnetic behaviors. The introduction of the Peierls potential in the DW model opens a path for a new explanation of the low temperature coercivity and influence of the field sweep rate measured in exchange biased FM/AFM bilayers.

ACKNOWLEDGMENTS

J.M. thanks Olivier Fruchart from Institut Néel for fruitful discussions.

[1] W. H. Meiklejohn and C. P. Bean, Phys. Rev. **102**, 1413 (1956).
[2] B. Dieny, V. S. Speriosu, S. Metin, S. S. P. Parkin, B. A. Gurney, P. Baumgart, and D. R. Wilhoit, J. Appl. Phys. **69**, 4774 (1991).
[3] W. H. Meiklejohn and C. P. Bean, Phys. Rev. **105**, 904 (1957).
[4] R. L. Stamps, J. Phys. D: Appl. Phys. **33**, R247 (2000).
[5] J. Nogués and I. K. Schuller, J. Magn. Magn. Mater. **192**, 203 (1999).
[6] A. E. Berkowitz and K. Takano, J. Magn. Magn. Mater. **200**, 552 (1999).
[7] M. Kiwi, J. Magn. Magn. Mater. **234**, 584 (2001).
[8] L. Néel, Ann. Phys. (Paris) **2**, 61 (1967).
[9] D. Mauri, H. C. Siegmann, P. S. Bagus, and E. Kay, J. Appl. Phys. **62**, 3047 (1987).
[10] A. P. Malozemoff, Phys. Rev. B **35**, 3679 (1987).
[11] D. Lederman, R. Ramirez, and M. Kiwi, Phys. Rev. B **70**, 184422 (2004).
[12] C. Mitsumata, A. Sakuma, and K. Fukamichi, Phys. Rev. B **68**, 014437 (2003).
[13] Z. Huang, S. Li, H. Lin, F. Zhang, and Y. Du, J. Magn. Magn. Mater. **303**, e180 (2006).
[14] N. C. Koon, Phys. Rev. Lett. **78**, 4865 (1997).
[15] T. C. Schulthess and W. H. Butler, Phys. Rev. Lett. **81**, 4516 (1998).
[16] U. Nowak, K. D. Usadel, J. Keller, P. Miltényi, B. Beschoten, and G. Güntherodt, Phys. Rev. B **66**, 014430 (2002).
[17] K. O'Grady, L. E. Fernandez-Outon, and G. Vallejo-Fernandez, J. Magn. Magn. Mater. **322**, 883 (2010).
[18] V. Baltz, G. Gaudin, P. Somani, and B. Dieny, Appl. Phys. Lett. **96**, 262505 (2010).
[19] E. Fulcomer and S. H. Charap, J. Appl. Phys. **43**, 4190 (1972).
[20] G. Vallejo-Fernandez, L. E. Fernandez-Outon, and K. O'Grady, J. Phys. D: Appl. Phys. **41**, 112001 (2008).

[21] D. Suess, M. Kirschner, T. Schrefl, W. Scholz, R. Dittrich, H. Forster, and J. Fidler, J. Appl. Phys. **93**, 8618 (2003).
[22] C. Leighton, J. Nogués, B. J. Jønsson-Åkerman, and I. K. Schuller, Phys. Rev. Lett. **84**, 3466 (2000).
[23] M. D. Stiles and R. D. McMichael, Phys. Rev. B **63**, 064405 (2001).
[24] M. D. Stiles and R. D. McMichael, Phys. Rev. B **59**, 3722 (1999).
[25] M. Ali, C. H. Marrows, M. Al-Jawad, B. J. Hickey, A. Misra, U. Nowak, and K. D. Usadel, Phys. Rev. B **68**, 214420 (2003).
[26] C. Hou, H. Fujiwara, K. Zhang, A. Tanaka, and Y. Shimizu, Phys. Rev. B **63**, 024411 (2000).
[27] T. Ambrose and C. L. Chien, J. Appl. Phys. **83**, 6822 (1998).
[28] H. R. Hilzinger and H. Kronmüller, Phys. Status Solidi B **54**, 593 (1972).
[29] T. Egami and C. D. Graham, J. Appl. Phys. **42**, 1299 (1971).
[30] B. Barbara, C. Bécle, R. Lemaire, and D. Paccard, J. Phys. Colloques **32**, C1-299 (1971).
[31] J. I. Arnaudas, A. Del Moral, and J. S. Abell, J. Magn. Magn. Mater. **61**, 370 (1986).
[32] H. Kronmüller, J. Magn. Magn. Mater. **7**, 341 (1978).
[33] J. Moritz, P. Bacher, and B. Dieny, Phys. Rev. Lett. **112**, 087201 (2014).
[34] B. Barbara, J. Magn. Magn. Mater. **129**, 79 (1994).
[35] B. Barbara, J. Phys. (Paris) **34**, 1039 (1973).
[36] J. Lajzerowicz and J. Niez, J. Phys. Lett. **40**, 165 (1979).
[37] H. Xi, R. M. White, S. Mao, Z. Gao, Z. Yang, and E. Murdock, Phys. Rev. B **64**, 184416 (2001).
[38] J. Moritz, S. van Dijken, and J. M. D. Coey, Eur. Phys. J. B **45**, 191 (2005).
[39] G. Malinowski, S. van Dijken, M. Czapkiewicz, and T. Stobiecki, Appl. Phys. Lett. **90**, 082501 (2007).
[40] K. Takano, R. H. Kodama, A. E. Berkowitz, W. Cao, and G. Thomas, Phys. Rev. Lett. **79**, 1130 (1997).
[41] B. Antonini and V. Minkiewicz, Solid State Commun. **10**, 203 (1972).
[42] N. P. Aley, R. Kroeger, B. Lafferty, J. Agnew, Y. Lu, and K. O'Grady, IEEE Trans. Magn. **45**, 3869 (2009).
[43] N. P. Aley, M. Bowes, R. Kroeger, and K. O'Grady, J. Appl. Phys. **107**, 09D722 (2010).